CONDENSED MATTER PHYSICS

Low-energy quasi-circular electron correlations with charge order wavelength in $Bi_2Sr_2CaCu_2O_{8+\delta}$

Kirsty Scott[1,2], Elliot Kisiel[3], Timothy J. Boyle[1,2,4], Rourav Basak[3], Gaëtan Jargot[5], Sarmistha Das[3], Stefano Agrestini[6], Mirian Garcia-Fernandez[6], Jaewon Choi[6], Jonathan Pelliciari[7], Jiemin Li[7], Yi-De Chuang[8], Ruidan Zhong[9]†, John A. Schneeloch[9]‡, Genda Gu[9], François Légaré[5], Alexander F. Kemper[10], Ke-Jin Zhou[6], Valentina Bisogni[7], Santiago Blanco-Canosa[11,12], Alex Frano[3,13], Fabio Boschini[5,14], Eduardo H. da Silva Neto[1,2,4,15]*

Most resonant inelastic x-ray scattering (RIXS) studies of dynamic charge order correlations in the cuprates have focused on the high-symmetry directions of the copper oxide plane. However, scattering along other in-plane directions should not be ignored as it may help understand, for example, the origin of charge order correlations or the isotropic scattering resulting in strange metal behavior. Our RIXS experiments reveal dynamic charge correlations over the q_x-q_y scattering plane in underdoped $Bi_2Sr_2CaCu_2O_{8+\delta}$. Tracking the softening of the RIXS-measured bond-stretching phonon, we show that these dynamic correlations exist at energies below approximately 70 meV and are centered around a quasi-circular manifold in the q_x-q_y scattering plane with radius equal to the magnitude of the charge order wave vector, q_{CO}. This phonon-tracking procedure also allows us to rule out fluctuations of short-range directional charge order (i.e., centered around [$q_x = \pm q_{CO}$, $q_y = 0$] and [$q_x = 0$, $q_y = \pm q_{CO}$]) as the origin of the observed correlations.

INTRODUCTION

Dynamic fluctuations from periodic charge order (CO) pervade the phase diagram of cuprate superconductors, perhaps even more than superconductivity itself (*1*). The detection of these fluctuations over energy and momentum was enabled by several recent advances in the energy resolution of resonant inelastic x-ray scattering (RIXS) instruments operating in the soft x-ray regime. In the case of $YBa_2Cu_3O_{6+\delta}$, Cu-L_3 RIXS detects dynamic correlations at the CO wave vector, q_{CO}, with a characteristic energy scale of approximately 20 meV (*2*). It has been proposed that these low-energy short-range dynamic CO correlations are a key ingredient to the strange metal behavior (*3*, *4*) characterized by linear-in-temperature resistivity (*5*, *6*). On one hand, this temperature behavior is often associated with an isotropic scattering rate that depends only on temperature in units of energy and Planck's constant (i.e., $\propto k_B T/\hbar$, sometimes called the Planckian regime) (*7*–*11*), as supported by recent angle-dependent magnetoresistance measurements of $La_{1.6-x}Nd_{0.4}Sr_xCuO_4$ (*12*). On the other hand, combined transport and RIXS studies have recently shown an unexpected link between linear-in-temperature resistivity and CO in $YBa_2Cu_3O_{6+\delta}$ (*13*, *14*). Combined, these latest results suggest that fluctuations of the CO should somehow result in an effective isotropic scattering. Still, high-resolution RIXS experiments have largely focused on the fluctuations along the high-symmetry crystallographic directions only, leaving the full structure of electron correlations within the copper oxide plane unknown.

Recently, in $Bi_2Sr_2CaCu_2O_{8+\delta}$ (Bi-2212), RIXS measurements found the existence of a quasi-circular pattern in the q_x-q_y plane at finite energies and with the same wave vector magnitude as that of the observed static CO peak at $\mathbf{q} = [q_x = \pm q_{CO}, q_y = 0]$ and $[q_x = 0, q_y = \pm q_{CO}]$—i.e., dynamic correlations with CO wavelength along all direction in the CuO_2 plane (*15*). Although the medium energy resolution of those measurements ($\Delta E \approx 0.8$ eV) precluded a more precise determination of their energy profile, the results suggested that these quasi-circular dynamic correlations (QCDCs) appear broad over the mid-infrared ranges (defined approximately as 100 to 900 meV). This scattering manifold, which may result from combined short- and long-range Coulomb interactions (*15*–*17*), would provide a large variety of wave vectors for connecting all points of the Fermi surface (i.e., an effective isotropic scattering). However, it is not yet experimentally known whether this manifold extends to electron scattering at lower energies, in the quasi-elastic regime. To experimentally investigate this scenario, we used high energy resolution (≈37 meV) Cu-L_3 RIXS q_x-q_y mapping of the electronic correlations in Bi-2212. Using the softening of the bond-stretching (BS) phonon in RIXS as a marker of CO correlations, our measurements reveal the presence of low-energy quasi-circular dynamic electronic correlations with $|\mathbf{q}| \approx q_{CO}$.

[1]Department of Physics, Yale University, New Haven, CT 06520, USA. [2]Energy Sciences Institute, Yale University, West Haven, CT 06516, USA. [3]Department of Physics, University of California San Diego, La Jolla, CA 92093, USA. [4]Department of Physics and Astronomy, University of California, Davis, CA 95616, USA. [5]Centre Énergie Matériaux Télécommunications, Institut National de la Recherche Scientifique, Varennes, Québec J3X 1S2, Canada. [6]Diamond Light Source, Harwell Campus, Didcot OX11 0DE, UK. [7]National Synchrotron Light Source II, Brookhaven National Laboratory, Upton, NY 11973, USA. [8]Advanced Light Source, Lawrence Berkeley National Laboratory, Berkeley, CA 94720, USA. [9]Condensed Matter Physics and Materials Science, Brookhaven National Laboratory, Upton, NY 11973, USA. [10]Department of Physics, North Carolina State University, Raleigh, NC 27695, USA. [11]Donostia International Physics Center (DIPC), 20018 Donostia–San Sebastian, Basque Country, Spain. [12]IKERBASQUE, Basque Foundation for Science, 48013 Bilbao, Spain. [13]Canadian Institute for Advanced Research, Toronto, ON M5G 1M1, Canada. [14]Quantum Matter Institute, University of British Columbia, Vancouver, BC V6T 1Z4, Canada. [15]Department of Applied Physics, Yale University, New Haven, CT 06520, USA.
*Corresponding author. Email: eduardo.dasilvaneto@yale.edu
†Present address: Tsung-Dao Lee Institute and School of Physics and Astronomy, Shanghai Jiao Tong University, Shanghai 200240, China.
‡Present address: Department of Physics, University of Virginia, Charlottesville, VA 22904, USA.

RESULTS

High-resolution RIXS mapping of dynamic correlations in the q_x-q_y plane

We performed Cu-L_3 RIXS measurements (approximately 931.5 eV incoming photon energy) at $\phi = 0°$, 25°, 30°, 35°, and 45°, where ϕ is defined as the azimuthal angle from the q_x axis. For each ϕ, we acquired RIXS spectra at different values of in-plane momentum transfer $q = |\mathbf{q}|$ by varying the incident angle on the sample. Throughout the paper, values of q are reported in reciprocal lattice units (r.l.u.), where 1 r.l.u. is defined as $2\pi/a$ and $a = 3.82$ Å (the lattice constant along $\phi = 0°$). The measurements were performed at $T = 60$ K, which is the superconducting transition temperature (T_c) for the measured sample, except for one measurement performed at $T = 25$ K below T_c. Supporting measurements on a similar sample ($T_c = 54$ K), shown in the Supplementary Materials, were performed at 54 K, except for one measurement at 300 K (Supplementary Materials, figs. S2 and S5). In Fig. 1 (A and B), we show representative spectra obtained at q near q_{CO} for $\phi = 0°$ and 30°, and energies below 1.1 eV. In these two cases, the minimal model that fits the data includes five contributions: a quasi-elastic peak, a BS phonon peak at ≈70 meV, a peak at ≈135 meV (likely from a two-phonon process), a broad paramagnon, and a broad background feature of unknown origin. A similar assessment can be made regarding all other high-resolution spectra acquired in this work. It may be the case that high-energy QCDCs (*15*) are somehow encompassed by the phenomenological background term of the fitting function. However, in this type of fitting analysis, it is generally difficult to disentangle overlapping contributions to the RIXS spectra using a fitting model with so many parameters, thus precluding the extraction of the exact spectral profile of the QCDCs with any reasonable confidence. Still, we note that these high-resolution data are consistent with the previously reported medium-resolution data (*15*), which can be verified by integration of the high-resolution data (see fig. S9).

From the above discussion, we consider the possibility that the spectral intensity of QCDCs in Bi-2212 is so dilute over energy as to preclude the reliable use of curve fitting algorithms for the extraction of their spectral structure amid stronger paramagnon and phonon signals. Instead, here we develop a different method to detect QCDCs at lower energies, by tracking the evolution of the BS phonon over the q_x-q_y plane. This method is based on the phenomenology revealed by several recent RIXS measurements of the cuprates along q_x and q_y, which indicate an apparent softening of the BS phonon peak at the momentum location of the static CO peak (*18*–*23*). The BS phonon is also an ideal probe of QCDCs because both its dispersion and electron-phonon coupling vary weakly as a function of ϕ in the absence of CO correlations (*24*, *25*). We call the procedure where we probe QCDCs with the BS phonon a phonon-tracking method and note that the softening of the BS phonon can be caused by either static or dynamic correlations. In the case of Bi-2212, it has been proposed that the apparent softening of the BS phonon in RIXS is due to an interplay between low-energy dynamic fluctuations of the CO and BS phonons that result in a Fano-like interference (*18*, *21*, *23*, *26*). Another possibility is that the apparent softening is simply the result of the phonon peak and a low-energy CO peak overlapping, as recently suggested by measurements of both $YBa_2Cu_3O_{6+\delta}$ and Bi-2212 (*27*). In either

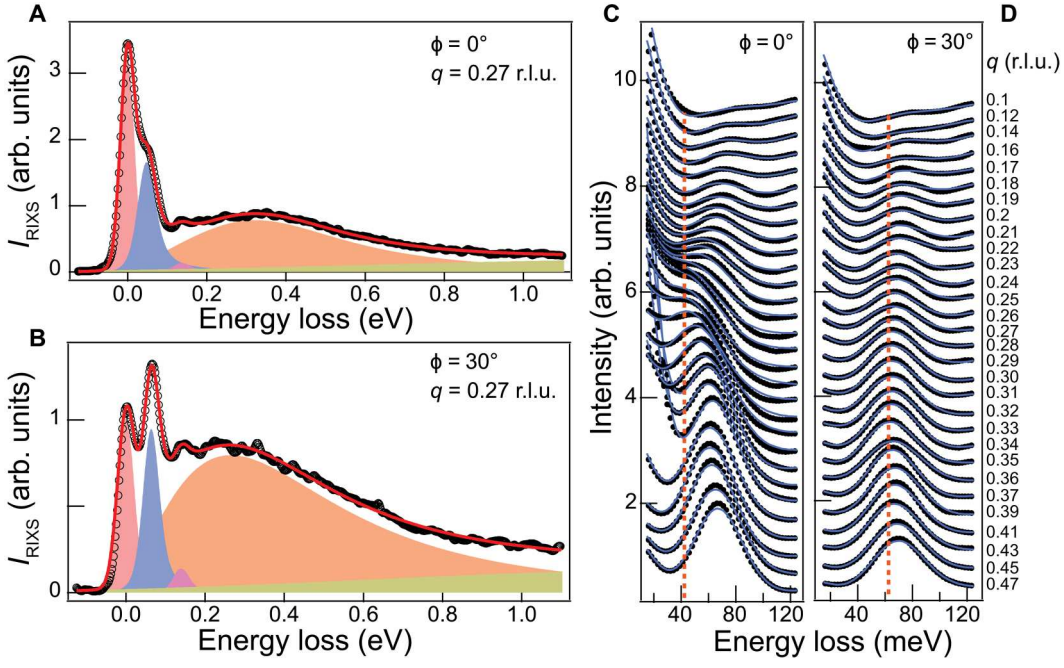

Fig. 1. RIXS spectra and fitting. (**A** and **B**) Examples of spectra at $q = 0.27$ r.l.u. for $\phi = 0°$ and 30°, respectively (open circles). The red lines are fits to the spectra, composed of a quasi-elastic peak (pink), a BS phonon peak at ≈70 meV (blue), a peak at ≈135 meV (likely from a two-phonon process) (purple), a broad paramagnon (orange), and a broad background feature of unknown origin (brown). (**C** and **D**) RIXS measured BS phonon peak for various values of q measured for $\phi = 0°$ and 30°, respectively (black circles). The blue lines are the fits to the spectra. The vertical orange dashed lines, indicating the lowest phonon peak position at each ϕ, are shown to help the reader observe the phonon dispersions in the raw data. r.l.u., reciprocal lattice units.

interpretation, the location of the phonon softening can be used as a marker for low-energy dynamic CO correlations.

Figure 1 (C and D) shows the spectra acquired as a function of q for $\phi = 0°$ and 30°, respectively, focusing on the region of the BS phonon. At $\phi = 0°$, it is clear that the phonon peak position softens to its lowest energy value at $q = q_{CO} \approx 0.29$ r.l.u. (Fig. 1C). Careful observation of the spectra taken along $\phi = 30°$ shows a similar softening effect with the lowest phonon energy position occurring for $q \approx q_{CO}$ (Fig. 1D). Figure 2A shows the mapping of the BS phonon mode at $\phi = 0°$ and 30° obtained after subtraction of the fitted elastic line, once again showing the softening of the RIXS phonon even at $\phi = 30°$. To precisely determine the locations of the softening in the q_x-q_y plane, we fit the spectra to extract the dispersion of the BS phonon for each ϕ (Fig. 2B). We observe a softening of the RIXS measured phonon line for all ϕ, except for $\phi = 45°$. All observed softening occurs at a value of $q \approx q_{CO}$, precisely as expected for QCDCs at low energies.

Discriminating QCDCs from short-range directional order

Dynamic correlations emanating from short-range order are bound to be broad in **q**. It is therefore reasonable to ask whether the measured q_x-q_y profile of the BS phonon could simply be the result of diffuse scattering from short-range directional order. The fundamental difference between QCDCs and short-range directional order is that the former forms a manifold of dynamic correlations centered at $q \approx q_{CO}$ [similar to Brazovskii-type fluctuations (*15*, *28*)], while the latter results in dynamic correlations around $\mathbf{q} = [q_x = \pm q_{CO}, q_y = 0]$ and $\mathbf{q} = [q_x = 0, q_y = \pm q_{CO}]$. To contrast these scenarios, we consider two simple toy models (more details on the toy models are provided in Materials and Methods). In both cases, we start with a flat $|\mathbf{q}|$-independent phonon mode at 72 meV, which is a reasonable approximation given the small dispersion of the BS phonon in the absence of CO (*25*). In the first model (M1), we construct the QCDCs scenario, where the q cuts for various ϕ always have a minimum located at $q = q_{CO}$ (Fig. 3, A and B). In the second model (M2), we consider the case where dynamic CO correlations emerge isotropically from static peaks at $[q_x = \pm q_{CO}, q_y = 0]$ and $[q_x = 0, q_y = \pm q_{CO}]$. The corresponding phonon profile is shown in Fig. 3 (C and D). To roughly emulate the data, we also introduce a ϕ-dependent softening magnitude in M1, which increases from $\phi = 0°$ to 45° (Fig. 3A). However, note that the magnitude of the softening depends on the amount of CO correlations and on the ϕ structure of the electron-phonon coupling, which is not precisely known experimentally or necessary for discerning the two scenarios. The q cuts show a qualitatively similar behavior in both models: a clear phonon softening at $\phi = 0°$ that continues to exist even as ϕ approaches 45°. However, in M2, the q location of the phonon minima clearly decreases with increasing ϕ from 0° to 45°. This comparison explains our selection of ϕ values for these studies: The experimental ability to differentiate between

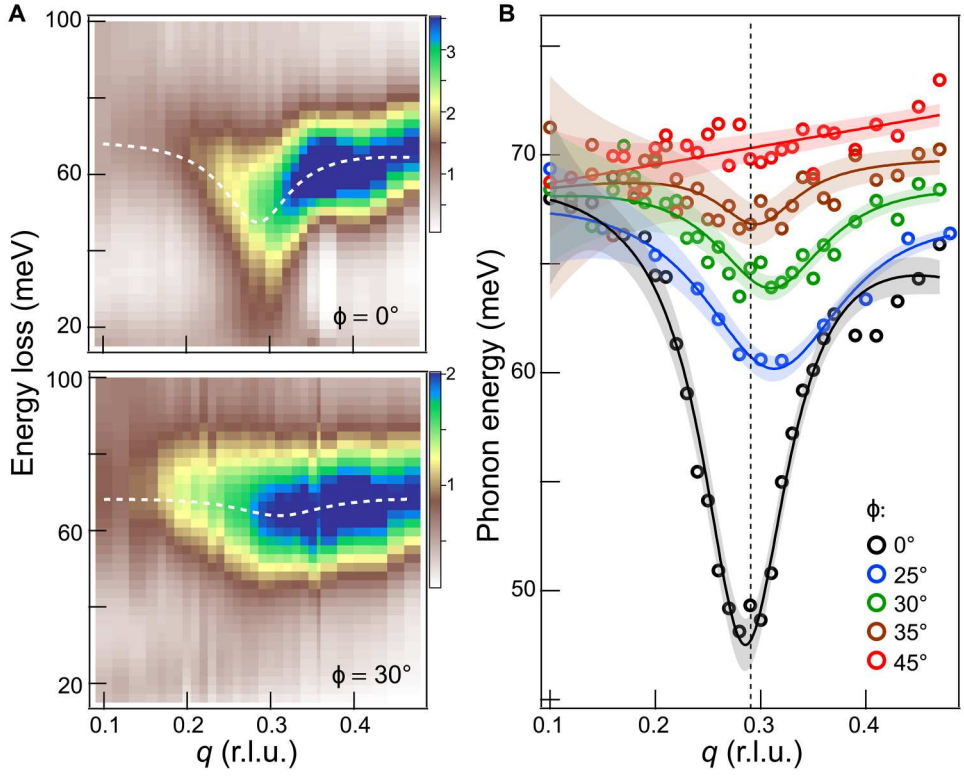

Fig. 2. Location of low-energy dynamic correlations extracted from the phonon dispersion. (**A**) Energy-momentum structure of the excitations at $\phi = 0°$ and 30° after subtraction of the elastic line. The image is constructed from RIXS spectra deconvoluted from the energy resolution. (**B**) Location of the phonon peak obtained by fitting the RIXS spectra deconvoluted from energy resolution for different ϕ (see Materials and Methods and also fig. S3). The solid lines are obtained by fitting the q dependence of the phonon peak (circles) with a negative Lorentzian function plus a linear background. The shaded regions around the solid lines are generated from the 95% confidence interval obtained for the various fits to the spectra (see Materials and Methods for details). The solid lines for $\phi = 0°$ and 30° in (B) appear as dashed white lines in (A). r.l.u., reciprocal lattice units.

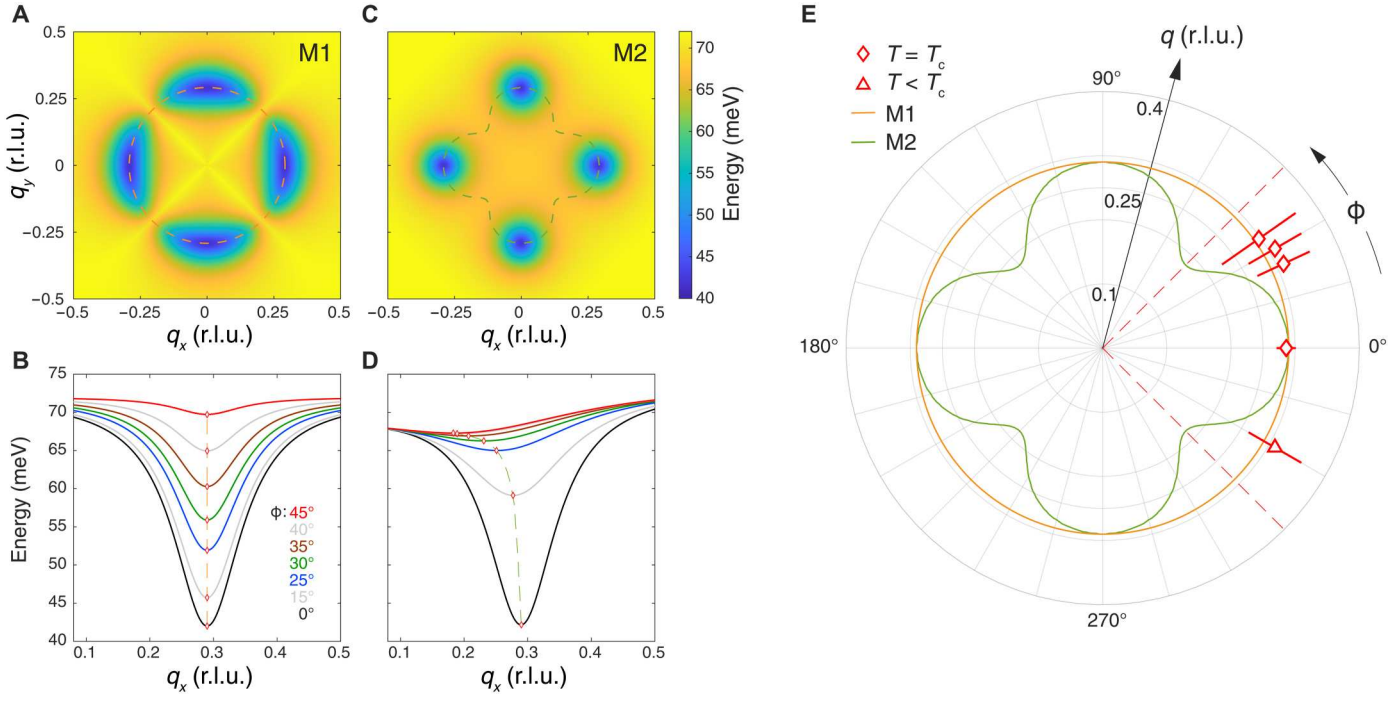

Fig. 3. Models of phonon softening for QCDCs and directional order. (**A** and **C**) Phonon dispersion for M1 and M2, as described in the text. (**B** and **D**) Momentum q cuts of the phonon dispersion at different ϕ for the simulated data in (A) and (C), respectively. The dashed orange and green lines in (A) to (D) identify the location of the phonon softening in the q_x-q_y plane. (**E**) Polar plot contrasting M1 and M2 models (orange and green solid lines) and the experimental data (red symbols). The error bars in (E) are obtained from the fits to the phonon dispersion in Fig. 2B. See Materials and Methods for more details. r.l.u., reciprocal lattice units.

M1 and M2 is largest in the ϕ = 25° to 45° range. The polar plot in Fig. 3E summarizes the analysis, comparing the q location of the minima for both models to the minima obtained from experiments (red markers with error bars). The experimental data are clearly consistent with M1, although deviations of M1 from a perfectly circular manifold (i.e., quasi-circular correlations) are possible within error bars. The comparison in Fig. 3E clearly rules out M2, the short-range directional order scenario, and instead indicates the quasi-circular nature of the low-energy correlations associated with the CO.

DISCUSSION

The experiments presented here provide evidence for the existence of QCDCs at low energies in underdoped Bi-2212, which could be a key ingredient for models that connect CO to an effective isotropic scattering. Long-range translational symmetry breaking cannot be responsible for this isotropy due to the characteristic length scale and directionality of the ordered state. Although short-range electron correlations from directional order, occupying a much larger region of momentum space, could, in principle, emulate isotropic scattering (*3*, *4*, *29*), the QCDCs revealed by our experiments offer a different scenario. Extending not only around the static CO wave vectors but also in the azimuthal direction, QCDCs might be a more viable platform for isotropic scattering. These QCDCs may also be related to the featureless continuum in the charge susceptibility observed by inelastic electron scattering, which has been discussed in connection to the marginal Fermi liquid hypothesis (*7*, *30*). To fully understand this possible relation and the impact of QCDCs to electronic properties of the cuprates, one requires knowledge of the energy structure of these correlations. Although this might still be beyond the current experimental capabilities, our experiments provide some constraints to the low-energy structure of the QCDCs. In particular, for the ϕ values where a softening is detected, QCDCs must exist below ≈70 meV (i.e., the approximate energy of the bare phonon). Given the weak ϕ dependence of the BS phonon coupling to electrons [see fig. S7 and (*24*)], the variations in the amount of energy softening observed from 0° to 45° likely reflect changes in the underlying CO correlations. Unfortunately, the amount of energy softening at $q = q_{CO}$ by itself, without precise knowledge of the ϕ-dependence of the electron-phonon interaction, does not provide more information about the energy structure of the QCDCs. Therefore, it remains possible that QCDCs at ϕ = 45° exist below 70 meV but do not substantially interact with the BS phonon.

To test for the presence of CO correlations even at ϕ = 45°, we analyzed the momentum dependence of the spectrum integrated over different energy windows (fig. S6, A and B). For ϕ ≥ 25°, including ϕ = 45°, we found a featureless momentum dependence when integrating around the elastic line, [− 10,10] meV. On the other hand, integration in a window between the elastic and phonon lines, [25,40] meV, reveals a broad maximum around q_{CO} even at ϕ = 45°. Given the 37 meV energy resolution of our RIXS measurements, we performed the same analysis over energy deconvoluted spectra (fig. S6, C and D) and obtained similar results. Although consistent with our phonon-tracking analysis, the energy integration analysis should be taken carefully because the integrated signal may also include contributions from low-energy phonons.

For this reason, it is also a less accurate indicator of the momentum structure of QCDCs when compared to the phonon-tracking method. Perhaps $q_x - q_y$ mapping by oxygen K edge RIXS measurements, which can reach resolutions better than 20 meV, may better resolve the low-energy structure of QCDCs and investigate their relation to the Planckian regime, akin to what has been done for La-based cuprates along $\phi = 0°$ (*31*). Together, the phonon-tracking analysis and the absence of a peak in the elastic channel near q_{CO} for $\phi \geq 25°$ establish the dynamic nature of the quasi-circular correlations.

Our experiments clearly reveal different manifolds for the static and low-energy dynamic correlations. While the static signal is confined to peaks centered around $[q_x = \pm q_{CO}, q_y = 0]$ and $[q_x = 0, q_y = \pm q_{CO}]$, the low-energy dynamic correlations form a quasi-circle in the q_x-q_y plane. This difference suggests that while, in principle, the QCDCs could condense into static order along any direction, the lattice constrains the static signal to a high-symmetry direction of the lattice. The quasi-circular shape of the low-energy correlations is also similar to the shape obtained from the analysis of higher-energy correlations [figs. S8 and S9 and (*15*)]. This similarity raises the possibility that the QCDCs exist up to much higher energies of the order of 1 eV. As discussed in (*15*), the quasi-circular correlations cannot be explained by an instability of the Fermi surface. Instead, it was proposed that the location of the dynamic CO correlations in **q**-space is determined by the minima of the effective Coulomb interaction, which becomes nonmonotonic in q due to the inclusion of a long-range Coulomb interaction. However, this nonmonotonic Coulomb interaction by itself failed to capture the intensity anisotropy observed at $q \approx q_{CO}$. Likewise, here the same proposed Coulomb interaction could also explain the most salient feature of our data, namely, the quasi-circular shape of the low-energy correlations. Recently, a more complete theoretical description based on a *t-J* model with long-range Coulomb interaction shows the presence of ring-like charge correlations with the correct intensity anisotropy (*17*). The results presented here can serve as a guide for future theoretical investigations that also account for the apparent decrease of the phonon softening from $\phi = 0°$ to 45°.

Beyond the fact that both the energy-integrated correlations (*15*) and the low-energy dynamic correlations appear to occupy the same quasi-circular scattering manifold, the current RIXS measurements do not provide further experimental evidence to connect the two phenomena. Comparing the two results, note that the analysis of the medium-resolution RIXS spectra of (*15*) relies on an energy window that also encompasses spin excitations known as paramagnons, which are centered around 300 meV near $q = q_{CO}$. Nonetheless, the paramagnons do not influence the dispersion anomaly of the BS phonon below ≈70 meV. An understanding of exactly how the low-energy QCDCs reported here connect to the high-energy correlations may come from polarimetric RIXS experiments that are able to decompose charge and spin excitations in the mid-infrared range, as has been done for electron-doped cuprates (*32*). In addition, compared to the energy-integration procedure, the phonon-tracking method provides higher precision for mapping CO correlations in the $q_x - q_y$ plane, because the large integration ranges required for the former result in very broad features in **q**-space. We have already performed medium-resolution RIXS measurements that detect the presence of similar quasi-circular scattering manifolds in the energy-integrated spectrum of optimally and overdoped samples, but the investigation of their doping dependence is hindered by the large experimental uncertainty associated with the integration method (see fig. S8). Instead, our procedure to track QCDCs using measurements of the RIXS BS phonon goes beyond demonstrating the existence of QCDCs in underdoped Bi-2212 at low energies. It is also a methodology that can be used to detect QCDCs in other cuprates and understand related phenomena such as the electron-doped cuprates, which also show a quasi-circular scattering (*33*). Last, the application of this method to multiple cuprate families at different dopings and/or temperatures will help unveil whether and how QCDCs and the strange metal are related.

MATERIALS AND METHODS

RIXS experiments

High-resolution RIXS experiments were performed at the I21 beamline (*34*) at Diamond Light Source, UK, and at the 2-ID beamline (*35*) at the National Synchrotron Light Source II, Brookhaven National Laboratory, USA. The orientation of the crystal axes of the underdoped $Bi_2Sr_2CaCu_2O_{8+\delta}$ samples was obtained by x-ray diffraction before the RIXS experiment. The samples were cleaved in air just moments before inserting them into the ultrahigh-vacuum chambers. For experiments at I21, the crystal was aligned to the scattering geometry in situfrom measurements of the 002 Bragg reflection and the *b*-axis superstructure peak. The scattering angle, 2θ, was fixed at 154° (I21) and 153° (2-ID). The fixed scattering angle setup, where q_z varies as a function of sample angle, is commonly used for Cu-L_3 RIXS on cuprates given the broad nature of CO correlations along q_z. Using $c = 30.8$ Å as the out-of-plane lattice constant, we obtain the $L = 3.83 \times 2\pi/c$ for the out-of-plane Miller index at an in-plane $q = 0.29 \times 2\pi/a$. The incoming light was set to vertical polarization (σ geometry) at the Cu-L_3 edge (≈931.5 eV). The combined energy resolution (full width at half maximum) was about 37 meV (I21) and 40 meV (2-ID), with small variations (±3 meV) over the course of multiple days. In both cases, the energy resolution was relaxed in a trade-off for intensity. The projection of the momentum transfer, q, in the q_x-q_y plane was obtained by varying the incident angle on the sample (θ). The momentum resolution depends on the geometry of the beamline and on the particular values of θ and 2θ. For the θ scans in this work, we find that the in-plane momentum resolution was better than $\pm 0.006 \times 2\pi/a$ (± 0.009 Å^{-1}) (*34*) at I21 and $\pm 0.002 \times 2\pi/a$ (± 0.004 Å^{-1}) (*35*), approximately. All the measurements were performed at $T = 60$ K (I21) or $T = 54$ K (2-ID), which are the superconducting transition temperatures for the measured samples, except for one measurement performed at $T = 25$ K below T_c (Fig. 3E; $T_c = 60$ K sample) and one measurement at 300 K (figs. S2 and S5; $T_c = 54$ K sample).

Analysis of RIXS spectra

To ensure the robustness of the extraction of phonon dispersion from the RIXS spectra, we analyzed the data using multiple methods. Although the overall RIXS cross section may depend on ϕ, we did not perform any normalization or intensity correction procedure to the spectra because the energy location of the phonon does not depend on the overall intensity. A comparison between the results for different methods is available in fig. S4.

Method 1

In an effort to maintain an agnostic approach and to not assume particular functional forms of the different contributions to the

RIXS spectra, we extracted the dispersion by simply tracking the energy positions of the phonon peak maximum in the RIXS spectra deconvoluted from the energy resolution. See below for details of the deconvolution procedure.

Method 2

The phonon dispersion shown in Fig. 2B was extracted by fitting the deconvoluted RIXS spectra (see Fig. 2A and fig. S3) in the [−30,130] meV range to a double Gaussian function plus a second-order polynomial background, keeping all parameters free. The shaded regions around the solid lines in Fig. 2B were generated by fitting the 95% confidence intervals (obtained from the fits) to a polynomial function of q.

Method 3

Following previous works (*23*, *36*), the raw RIXS spectra were fit to a five-component model that includes a Gaussian (elastic peak of amplitude A_{el}, position ω_{el}, and width w_{el}), two anti-Lorentzians (phonon and double-phonon peaks of different amplitude A_i and position ω_i, and sharing width w_{ph} and Fano parameter width q_F—note that i = 1,2 indicates the first and second phonon, respectively), a damped harmonic oscillator line shape (paramagnon of amplitude A_{pm}, position ω_{pm}, and damping parameter γ_{pm}), and an error function (smooth background described by an error function with amplitude A_{BG}, position ω_{BG}, and width w_{BG})

$$f(\omega) = A_{el}e^{-\frac{(\omega-\omega_{el})^2}{w_{el}^2}} + \sum_{i=1,2} A_i \frac{2(\omega-\omega_i)/w_{ph}+q_F}{[2(\omega-\omega_i)/w_{ph}]^2+1} + \\ + A_{pm}\frac{\gamma_{pm}\omega}{(\omega^2-\omega_{pm}^2)^2+4\gamma_{pm}^2\omega^2} + A_{BG}\left[\mathrm{erf}\left(\frac{\omega-\omega_{BG}}{w_{BG}}\right)+1\right] \quad (1)$$

The fitting model is convoluted with the RIXS energy resolution (~37 meV). From this analysis, we extracted the phonon dispersion for each ϕ that quantitatively matches the phonon dispersion shown in Fig. 2B. All parameters are kept free, except for ω_{BG}, which is constrained within a range of [0.2,0.6] eV.

Fitting the phonon dispersion

To obtain a phenomenological form to the dispersions in Fig. 2B, the extracted peak locations as a function of q were fit to a linear background plus a negative Lorentzian function. From this fit, we obtain the q location of the softening (red markers in Fig. 3E). To obtain the error bars in Fig. 3E, we follow a conservative approach by taking the average of the two q intercepts of the fitted curve at E_{min} + 2 meV, where E_{min} is the lowest energy of the dispersion and ±2 meV is the typical amount of scatter observed in the data. For ϕ = 45°, the data are fit to a line.

Deconvolution procedure

We used the Lucy-Richardson deconvolution procedure (*37*) to deconvolve the energy resolution (~37 meV) from the RIXS spectra (deconvoluted curves for all azimuths are displayed in fig. S3). The number of iterations and region of interest of the deconvolution procedure were optimized by ensuring that the convolution of the deconvoluted curves reproduced the raw data.

Model simulations

The toy models M1 and M2 are purely phenomenological. For M1, the phonon dispersion was modeled as

$$E = E_0 - \xi(\phi)\frac{\Delta}{\left(\frac{q-q_0}{\Gamma}\right)^2+1} \quad (2)$$

where E_0 = 72 meV, Δ = 30 meV, Γ = 0.065 r.l.u., q_0 = 0.29 r.l.u., and ξ(ϕ) = (|cos (2ϕ)| + 0.08)/(1.08). For M2, the phonon dispersion was modeled as

$$E = E_0 - \sum_{i=1}^{4}\frac{\Delta}{\left(\frac{\mathbf{q}-\mathbf{q}_i}{\Gamma}\right)^2+1} \quad (3)$$

where E_0 = 74 meV, Δ = 30 meV, Γ = 0.065 r.l.u., and $\mathbf{q}_i$ are the four peaks located at [$q_x = \pm q_{CO}$, $q_y = 0$] and [$q_x = 0$, $q_y = \pm q_{CO}$] (q_{CO} = 0.29 r.l.u.).

Supplementary Materials

This PDF file includes:

Figs. S1 to S11

Connection between low- and high-energy QCDCs

REFERENCES AND NOTES

1. R. Arpaia, G. Ghiringhelli, Charge order at high temperature in cuprate superconductors. *J. Physical Soc. Japan* **90**, 111005 (2021).
2. R. Arpaia, S. Caprara, R. Fumagalli, G. De Vecchi, Y. Y. Peng, E. Andersson, D. Betto, G. M. De Luca, N. B. Brookes, F. Lombardi, M. Salluzzo, L. Braicovich, C. Di Castro, M. Grilli, G. Ghiringhelli, Dynamical charge density fluctuations pervading the phase diagram of a Cu-based high-T_c superconductor. *Science* **365**, 906–910 (2019).
3. G. Seibold, R. Arpaia, Y. Y. Peng, R. Fumagalli, L. Braicovich, C. Di Castro, M. Grilli, G. C. Ghiringhelli, S. Caprara, Strange metal behaviour from charge density fluctuations in cuprates. *Commun. Phys.* **4**, 7 (2021).
4. S. Caprara, C. D. Castro, G. Mirarchi, G. Seibold, M. Grilli, Dissipation-driven strange metal behavior. *Commun. Phys.* **5**, 10 (2022).
5. M. Gurvitch, A. T. Fiory, Resistivity of $La_{1.825}Sr_{0.175}CuO_4$ and $YBa_2Cu_3O_7$ to 1100 K: Absence of saturation and its implications. *Phys. Rev. Lett.* **59**, 1337–1340 (1987).
6. S. Martin, A. T. Fiory, R. M. Fleming, L. F. Schneemeyer, J. V. Waszczak, Normal-state transport properties of $Bi_{2+x}Sr_{2-y}CuO_{6+\delta}$ crystals. *Phys. Rev. B Condens. Matter* **41**, 846–849 (1990).
7. C. M. Varma, P. B. Littlewood, S. Schmitt-Rink, E. Abrahams, A. E. Ruckenstein, Phenomenology of the normal state of Cu-O high-temperature superconductors. *Phys. Rev. Lett.* **63**, 1996–1999 (1989).
8. V. Aji, C. M. Varma, Theory of the quantum critical fluctuations in cuprate superconductors. *Phys. Rev. Lett.* **99**, 067003 (2007).
9. A. A. Patel, J. McGreevy, D. P. Arovas, S. Sachdev, Magnetotransport in a model of a disordered strange metal. *Phys. Rev. X* **8**, 021049 (2018).
10. A. A. Patel, S. Sachdev, Theory of a Planckian metal. *Phys. Rev. Lett.* **123**, 066601 (2019).
11. P. W. Phillips, N. E. Hussey, P. Abbamonte, Stranger than metals. *Science* **377**, eabh4273 (2022).
12. G. Grissonnanche, Y. Fang, A. Legros, S. Verret, F. Laliberté, C. Collignon, J. Zhou, D. Graf, P. A. Goddard, L. Taillefer, B. J. Ramshaw, Linear-in temperature resistivity from an isotropic Planckian scattering rate. *Nature* **595**, 667–672 (2021).
13. E. Wahlberg, R. Arpaia, G. Seibold, M. Rossi, R. Fumagalli, E. Trabaldo, N. B. Brookes, L. Braicovich, S. Caprara, U. Gran, G. Ghiringhelli, T. Bauch, F. Lombardi, Restored strange metal phase through suppression of charge density waves in underdoped $YBa_2Cu_3O_{7-\delta}$. *Science* **373**, 1506–1510 (2021).
14. M. Le Tacon, Strange bedfellows inside a superconductor. *Science* **373**, 1438–1439 (2021).
15. F. Boschini, M. Minola, R. Sutarto, E. Schierle, M. Bluschke, S. Das, Y. Yang, M. Michiardi, Y. C. Shao, X. Feng, S. Ono, R. D. Zhong, J. A. Schneeloch, G. D. Gu, E. Weschke, F. He, Y. D. Chuang, B. Keimer, A. Damascelli, A. Frano, E. H. da Silva Neto, Dynamic electron correlations with charge order wavelength along all directions in the copper oxide plane. *Nat. Commun.* **12**, 597 (2021).

16. H. Yamase, M. Bejas, A. Greco, Electron self-energy from quantum charge fluctuations in the layered $t - J$ model with long-range Coulomb interaction. *Phys. Rev. B* **104**, 045141 (2021).
17. M. Bejas, R. Zeyher, A. Greco, Ring-like shaped charge modulations in the $t - J$ model with long-range Coulomb interaction. *Phys. Rev. B* **106**, 224512 (2022).
18. L. Chaix, G. Ghiringhelli, Y. Y. Peng, M. Hashimoto, B. Moritz, K. Kummer, N. B. Brookes, Y. He, S. Chen, S. Ishida, Y. Yoshida, H. Eisaki, M. Salluzzo, L. Braicovich, Z.-X. Shen, T. P. Devereaux, W.-S. Lee, Dispersive charge density wave excitations in $Bi_2Sr_2\ CaCu_2O_{8+\delta}$. *Nat. Phys.* **13**, 952–956 (2017).
19. J. Q. Lin, H. Miao, D. G. Mazzone, G. D. Gu, A. Nag, A. C. Walters, M. Garcia-Fernández, A. Barbour, J. Pelliciari, I. Jarrige, M. Oda, K. Kurosawa, N. Momono, K.-J. Zhou, V. Bisogni, X. Liu, M. P. M. Dean, Strongly correlated charge density wave in $La_{2-x}Sr_xCuO_4$ evidenced by doping-dependent phonon anomaly. *Phys. Rev. Lett.* **124**, 207005 (2020).
20. Y. Y. Peng, A. A. Husain, M. Mitrano, S. X.-L. Sun, T. A. Johnson, A. V. Zakrzewski, G. J. MacDougall, A. Barbour, I. Jarrige, V. Bisogni, P. Abbamonte, Enhanced electron-phonon coupling for charge-density-wave formation in $La_{1.8-x}Eu_{0.2}Sr_xCuO_{4+\delta}$. *Phys. Rev. Lett.* **125**, 097002 (2020).
21. J. Li, A. Nag, J. Pelliciari, H. Robarts, A. Walters, M. Garcia-Fernandez, H. Eisaki, D. Song, H. Ding, S. Johnston, R. Comin, K.-J. Zhou, Multiorbital charge-density wave excitations and concomitant phonon anomalies in $Bi_2Sr_2\ LaCuO_{6+\delta}$. *Proc. Natl. Acad. Sci. U.S.A.* **117**, 16219–16225 (2020).
22. Q. Wang, K. von Arx, M. Horio, D. J. Mukkattukavil, J. Küspert, Y. Sassa, T. Schmitt, A. Nag, S. Pyon, T. Takayama, H. Takagi, M. Garcia-Fernandez, K.-J. Zhou, J. Chang, Charge order lock-in by electron-phonon coupling in $La_{1.675}Eu_{0.2}\ Sr_{0.125}\ CuO_4$. *Sci. Adv.* **7**, eabg7394 (2021).
23. W. S. Lee, K.-J. Zhou, M. Hepting, J. Li, A. Nag, A. C. Walters, M. Garcia-Fernandez, H. C. Robarts, M. Hashimoto, H. Lu, B. Nosarzewski, D. Song, H. Eisaki, Z. X. Shen, B. Moritz, J. Zaanen, T. P. Devereaux, Spectroscopic fingerprint of charge order melting driven by quantum fluctuations in a cuprate. *Nat. Phys.* **17**, 53–57 (2021).
24. S. Johnston, F. Vernay, B. Moritz, Z.-X. Shen, N. Nagaosa, J. Zaanen, T. P. Devereaux, Systematic study of electron-phonon coupling to oxygen modes across the cuprates. *Phys. Rev. B* **82**, 064513 (2010).
25. L. Braicovich, M. Rossi, R. Fumagalli, Y. Peng, Y. Wang, R. Arpaia, D. Betto, G. M. De Luca, D. Di Castro, K. Kummer, M. Moretti Sala, M. Pagetti, G. Balestrino, N. B. Brookes, M. Salluzzo, S. Johnston, J. van den Brink, G. Ghiringhelli, Determining the electron-phonon coupling in superconducting cuprates by resonant inelastic x-ray scattering: Methods and results on $Nd_{1+x}\ Ba_{2-x}\ Cu_3\ O_{7-\delta}$. *Phys. Rev. Res.* **2**, 023231 (2020).
26. H. Lu, M. Hashimoto, S.-D. Chen, S. Ishida, D. Song, H. Eisaki, A. Nag, M. Garcia-Fernandez, R. Arpaia, G. Ghiringhelli, L. Braicovich, J. Zaanen, B. Moritz, K. Kummer, N. B. Brookes, K.-J. Zhou, Z.-X. Shen, T. P. Devereaux, W.-S. Lee, Identification of a characteristic doping for charge order phenomena in Bi-2212 cuprates via RIXS. *Phys. Rev. B* **106**, 155109 (2022).
27. R. Arpaia, L. Martinelli, M. M. Sala, S. Caprara, A. Nag, N. B. Brookes, P. Camisa, Q. Li, Q. Gao, X. Zhou, M. Garcia-Fernandez, K. J. Zhou, E. Schierle, T. Bauch, Y. Y. Peng, C. Di Castro, M. Grilli, F. Lombardi, L. Braicovich, G. Ghiringhelli, Signature of quantum criticality in cuprates by charge density fluctuations. *arXiv* **2208**, 13918 (2022).
28. S. A. Brazovskii, Phase transition of an isotropic system to a nonuniform state. *Sov. Phys. JETP* **41**, 85–89 (1974).
29. A. Abanov, A. V. Chubukov, J. Schmalian, Quantum-critical theory of the spin-fermion model and its application to cuprates: Normal state analysis. *Adv. Phys.* **52**, 119–218 (2003).
30. M. Mitrano, A. A. Husain, S. Vig, A. Kogar, M. S. Rak, S. I. Rubeck, J. Schmalian, B. Uchoa, J. Schneeloch, R. Zhong, G. D. Gu, P. Abbamonte, Anomalous density fluctuations in a strange metal. *Proc. Natl. Acad. Sci.* **115**, 5392–5396 (2018).
31. H. Y. Huang, A. Singh, C. Y. Mou, S. Johnston, A. F. Kemper, J. van den Brink, P. J. Chen, T. K. Lee, J. Okamoto, Y. Y. Chu, J. H. Li, S. Komiya, A. C. Komarek, A. Fujimori, C. T. Chen, D. J. Huang, Quantum fluctuations of charge order induce phonon softening in a superconducting cuprate. *Phys. Rev. X* **11**, 041038 (2021).
32. E. H. da Silva Neto, M. Minola, B. Yu, W. Tabis, M. Bluschke, D. Unruh, H. Suzuki, Y. Li, G. Yu, D. Betto, K. Kummer, F. Yakhou, N. B. Brookes, M. Le Tacon, M. Greven, B. Keimer, A. Damascelli, Coupling between dynamic magnetic and charge-order correlations in the cuprate superconductor $Nd_{2-x}\ Ce_x\ CuO_4$. *Phys. Rev. B* **98**, 161114 (2018).
33. M. Kang, J. Pelliciari, A. Frano, N. Breznay, E. Schierle, E. Weschke, R. Sutarto, F. He, P. Shafer, E. Arenholz, M. Chen, K. Zhang, A. Ruiz, Z. Hao, S. Lewin, J. Analytis, Y. Krockenberger, H. Yamamoto, T. Das, R. Comin, Evolution of charge order topology across a magnetic phase transition in cuprate superconductors. *Nat. Phys.* **15**, 335–340 (2019).
34. K.-J. Zhou, A. Walters, M. Garcia-Fernandez, T. Rice, M. Hand, A. Nag, J. Li, S. Agrestini, P. Garland, H. Wang, S. Alcock, I. Nistea, B. Nutter, N. Rubies, G. Knap, M. Gaughran, F. Yuan, P. Chang, J. Emmins, G. Howell, I21: An advanced high-resolution resonant inelastic X-ray scattering beamline at Diamond Light Source. *J. Synchrotron. Radiat.* **29**, 563–580 (2022).
35. J. Dvorak, I. Jarrige, V. Bisogni, S. Coburn, W. Leonhardt, Towards 10 meV resolution: The design of an ultrahigh resolution soft X-ray RIXS spectrometer. *Rev. Sci. Instrum.* **87**, 115109 (2016).
36. L. Wang, G. He, Z. Yang, M. Garcia-Fernandez, A. Nag, K. Zhou, M. Minola, M. L. Tacon, B. Keimer, Y. Peng, Y. Li, Paramagnons and high-temperature superconductivity in a model family of cuprates. *Nat. Commun.* **13**, 3163 (2022).
37. H.-B. Yang, J. D. Rameau, P. D. Johnson, T. Valla, A. Tsvelik, G. D. Gu, Emergence of preformed Cooper pairs from the doped Mott insulating state in $Bi_2\ Sr_2\ CaCu_2O_{8+\delta}$. *Nature* **456**, 77–80 (2008).
38. K. Scott, E. Kisiel, T. J. Boyle, R. Basak, G. Jargot, S. Das, S. Agrestini, M. Garcia-Fernandez, J. Choi, J. Pelliciari, J. Li, Y. D. Chuang, R. D. Zhong, J. A. Schneeloch, G. D. Gu, F. Légaré, A. F. Kemper, K.-J. Zhou, V. Bisogni, S. Blanco-Canosa, A. Frano, F. Boschini, E. H. da Silva Neto, Data from "Low-energy quasi-circular electron correlations with charge order wavelength in Bi2212".(2023).

Acknowledgments: We acknowledge the Diamond Light Source for time on beamline I21-RIXS under proposals MM28523 and MM30146. We especially acknowledge the incredible work done by the beamline staffs at I-21, 2-ID, and at 8.0.1 qRIXS, allowing many of these experiments to be performed remotely during the COVID pandemic. We thank A. Gozar for discussions during the preparation of this manuscript. **Funding:** This research used resources of the Advanced Light Source, a U.S. Department of Energy (DOE) Office of Science User Facility under contract no. DE-AC02-05CH11231. This research used beamline 2-ID of the National Synchrotron Light Source II, a DOE Office of Science User Facility operated for the DOE Office of Science by Brookhaven National Laboratory under contract no. DE-SC0012704. This work was supported by the Alfred P. Sloan Fellowship (E.H.d.S.N.). E.H.d.S.N. acknowledges support by the NSF under grant no. 2034345. A.F.K. was supported by the NSF under grant no. DMR-1752713. F.B. acknowledges support from the Fonds de recherche du Québec–Nature et technologies (FRQNT) and the Natural Sciences and Engineering Research Council of Canada (NSERC). A.F. was supported by the Research Corporation for Science Advancement via the Cottrell Scholar Award (27551) and the CIFAR Azrieli Global Scholars program. This material is based on work supported by the NSF under grant no. DMR-2145080. The synthesis work at Brookhaven National Laboratory was supported by the U.S. Department of Energy, Office of Basic Energy Sciences, contract no. DOE-SC0012704. **Author contributions:** E.H.d.S.N., F.B., and A.F. conceived the experiments. K.S., E.K., S.A., M.G.-F., V.B., K.-J.Z., J.C., T.J.B., R.B., Y.-D.C., A.F., F.B., and E.H.d.S.N. performed the RIXS experiments with the assistance of G.J., S.D., J.P., J.L., and F.L. R.Z., J.A.S., and G.D.G. synthesized and characterized the materials. K.S., T.J.B., R.B., F.B., and E.H.d.S.N. performed the analysis of the RIXS data. E.H.d.S.N., F.B., A.F., K.S., A.F.K., and S.B.-C. discussed and developed the interpretation of the data and contributed to the manuscript. E.H.d.S.N., F.B., A.F., and K.S. wrote the manuscript. All authors read and commented on the manuscript. E.H.d.S.N. was responsible for overall project direction, planning, and management. **Competing interests:** The authors declare that they have no competing interests. **Data and materials availability:** All data needed to evaluate the conclusions in the paper are present in the paper and/or the Supplementary Materials. The raw RIXS data underlying the results are available at the Dataverse repository: https://doi.org/10.7910/DVN/XB62JV (*38*).

Submitted 24 December 2022
Accepted 16 June 2023
Published 19 July 2023
10.1126/sciadv.adg3710

ScienceAdvances

Low-energy quasi-circular electron correlations with charge order wavelength in $Bi_2Sr_2CaCu_2O_{8+\#}$

Kirsty Scott, Elliot Kisiel, Timothy J. Boyle, Rourav Basak, Gaëtan Jargot, Sarmistha Das, Stefano Agrestini, Mirian Garcia-Fernandez, Jaewon Choi, Jonathan Pelliciari, Jiemin Li, Yi-De Chuang, Ruidan Zhong, John A. Schneeloch, Genda Gu, François Légaré, Alexander F. Kemper, Ke-Jin Zhou, Valentina Bisogni, Santiago Blanco-Canosa, Alex Frano, Fabio Boschini, and Eduardo H. da Silva Neto

Sci. Adv. **9** (29), eadg3710. DOI: 10.1126/sciadv.adg3710

Science Advances (ISSN 2375-2548) is published by the American Association for the Advancement of Science. 1200 New York Avenue NW, Washington, DC 20005. The title *Science Advances* is a registered trademark of AAAS.